

(U) Signal Separation and Localization Strategies for Large Aperture Acoustic Arrays

September 2017

Richard Haskins¹, Chris Simpson¹, Mihan McKenna¹

¹U.S. Army Engineer Research and Development Center
3909 Halls Ferry Road, Bldg. 5014
Vicksburg, MS 39180

ABSTRACT

(U) Development of signal detection and localization methods for large aperture acoustic arrays in urban environments presents inherent difficulties due in part to interfering coherent signals and low Signal to Noise Ratio (SNR) targets. Continuous wave sources can also be difficult to localize due to the high levels of self-similarity and interference with other continuous wave signals. This paper presents some preliminary approaches under investigation for: determining the direction of arrival of continuous sources that are changing in frequency, detecting and localizing low SNR impulses in the presence of coherent noise, and fast efficient mapping of array element delays to direction of arrival using a neural network fitting function.

(U) In the first part of this paper an approach for low level impulse detection is presented. This low SNR approach for weak impulse detection in the presence of local continuous noise monitors the linear estimated slope and offset of the spectral noise floor in a sliding window approach to detect a broadband or impulsive signal presence. This multistage process ignores strong continuous signals by clipping them from the fitting window and then detects the spectral domain ramps produced by short duration broadband impulses. This approach has also been extended to include recursive narrowband adaptive filtering and Independent Component Analysis. A brief discussion and some results from an automated neural network based fitting function that quickly maps array channel delays to azimuth and elevation direction of arrival (DOA) results is then presented. A simple scheme that automates the generation of this fitting function using Matlab tools is described. This section concludes with demonstration of impulse triangulation between arrays using the resolved direction of arrivals, as this is the ultimate goal for targets of interest when two or more SIAM arrays have detected the same source.

(U) The second part of this paper is focused on determining the direction of arrival for continuous sources. An ad-hoc cross-correlation modification is presented and demonstrated for localizing continuous sources that fail with standard short time cross-correlations due to improper phase cycle locking on the continuous source signal and a general lack of signal variability in the short time analysis window. After that, the use of relative frequency analysis for direction of arrival estimation is

presented. This method provides an alternative means of source localization other than beamforming or cross-correlation that is applicable to the analysis of frequency chirps due to either equipment state changes and/or Doppler chirps. The propagation of frequency changes across the array aperture can be characterized by means of the relative phase angle's rate of change or the relative instantaneous frequency. In this approach implemented in similar forms elsewhere [1][2] the outer array element's phase angles are referenced against the central reference array element to determine the source's direction of arrival. Examples demonstrating this approach on field data are presented at the end of this paper.

Permission to publish was granted by Director, Geotechnical and Structures Laboratory.

(U) 1 Introduction:

Impulses with higher signal to noise ratios are relatively easy to localize using multiple acoustic arrays. As coherent and non-coherent noise sources increase in intensity and proximity to arrays and as impulses get weaker due to size, location, weather, and topography, increased signal processing is typically required to recover and localize these various sources within the deployed environment. The recent Portuguese Dam experiments provide an example of the local interfering noise problem when noise from cars passing on the eastward highway reflected back at the receiving arrays from the mountain face abutting the Dam. Steering the array beam towards the dam from several of the arrays also captured the acoustic reflections of the traffic on this nearby highway.

(U) A primary goal of the work presented here is aimed at detection, localization, and classification (DLC) of sources of interest in the deployed environment. Even with coherent nuisance acoustic sources such as transformers, sump pumps, and highways, it is still important to characterize, localize and identify them for purposes such as false alarm decision making, unwanted spectral contribution filtering, null-beam steering, comb filters, and other optimization strategies related to regional monitoring goals. A comprehensive understanding of the local array's deployment environment and its typical sources and

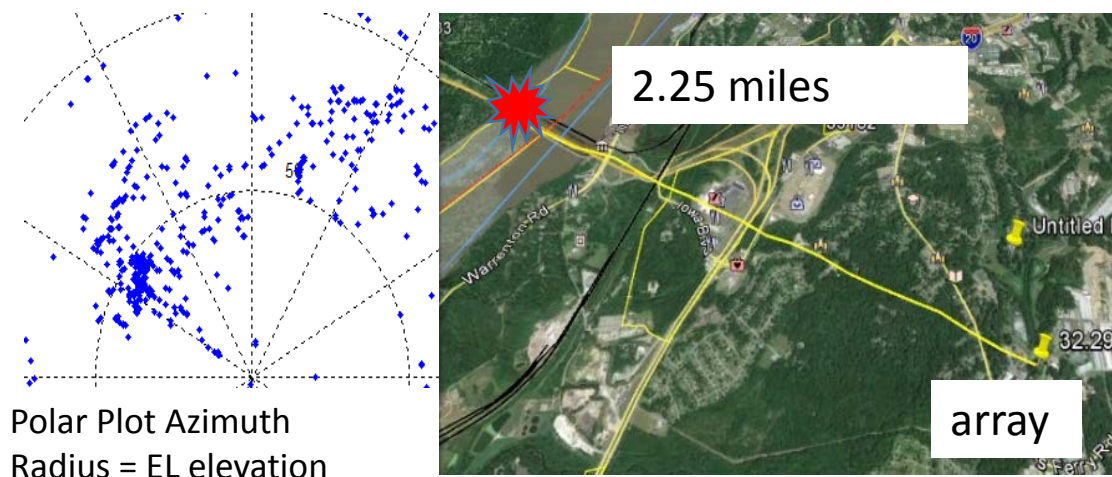


Figure 1 (U) Direction of arrival to the ERDC Vicksburg DAMES array from the MS River Barge Impact. left graph is direction of arrival for coherent detections over the time of the event and bottom right image shows an aerial map from the array to the impact location.

locations is key to acquiring and interpreting weaker and more challenging distant sources and the identification of unique events of interest. An example of one such non-typical event was captured during a high water event on the Mississippi River, when a barge train struck a bridge pier in 2017. This event was collected with the ERDC DAMES array. The Denied-Area Monitoring and Exploitation of Structures (DAMES) Array is a 1.8 kilometer aperture array of seismometers, strong motion gauges, audible acoustic microphones, infrasound and meteorological sensors including a ceilometer and weather balloon launching station, with a nested tactical 40 meter SIAM Array (Seismic-Infrasound-Audible Acoustic-Meteorological Array). The SIAM array components discussed in this paper are the five infrasound sensors oriented in a 'plus' geometry with a 60 meter array diameter with each of the four elements located on the magnetic compass axis and the and the first or default reference channel in the center. Shown in the bottom of figure 1 are detections from the sustained acoustic event of the barge train breaking apart and contacting itself and the bridge pier during the event. Following the first initial detections, multipath reflections from an adjacent building face were also present at approximately 30 degrees azimuth. Detections were considered coherent and retained when the focused signal had high correlation coefficients and a significant fraction of the energy was retained in the focused signal. Figure 2 (top) shows a typical time versus frequency STFT image in an urban environment. In this particular STFT the array is focused on the strongest correlated sources present at each time instance (red lines in image). By integrating urban detections and determining their direction of arrivals activity maps such as the one shown in the bottom of Figure 2 can be generated. This elevation vs azimuth plot is from 20 minutes of detection data and varies significantly depending on time of day and regional activity. It can be useful in determining directions more subject to interference, time and space variations of local noise sources. Some general inferences can be made as well. Sources on the map with zero elevation are more likely to be topographically line-of-sight, while sources who extend over Signiant low to high elevations are likely major sources such as busy roads. In general this map provides feedback via the detected coherent signals on regional coherent noise sources over various observational time windows. Detection distance or range will also vary according to the source's intensity, frequency content, topography, atmospheric conditions, and processing methods used. These two images in Figure 2 are presented to help illustrate the complexity of the urban acoustic environment and the need for detailed analysis tools to improve source characterization and separation.

(U) The work presented here starts with weak impulses in the presence of local background noise. Efficient detection and localization strategies are discussed before going into several localization approaches for continuous sources.

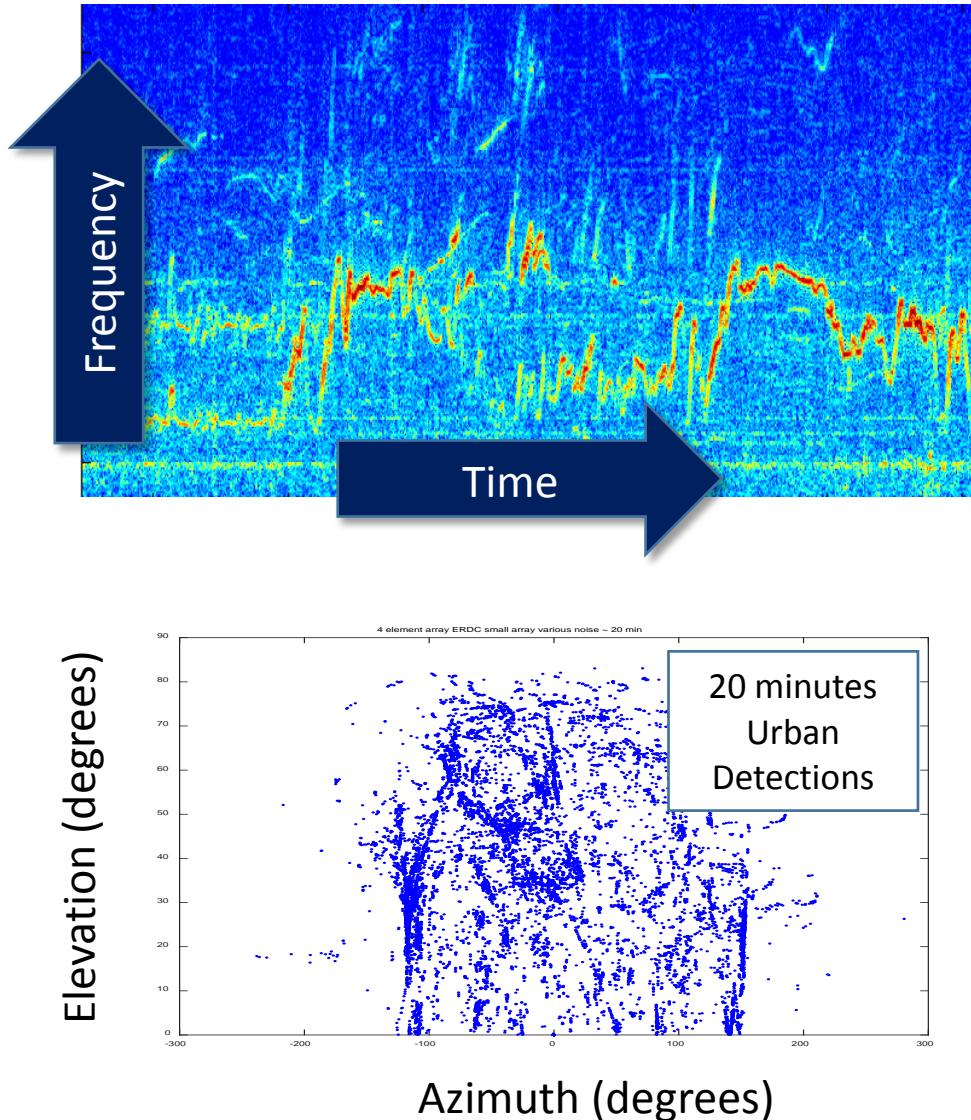


Figure 2. (U) Example Short time frequency transform showing typical time varying frequencies received in an urban environment. Note the significant number of sources and harmonics present at once. Red lines indicate the strongest correlated signal present at each time instant. (Bottom) Detection activity map plotted as elevation vs azimuth DOA for 20 minutes of activity in an urban environment.

(U) 2.1 Weak Impulses in the presence of continuous noise:

(U) Local continuous harmonic noise sources are often experienced in proximity to SIAM arrays deployed in or near urban environments. These can include: generators, transformers, air conditioning units, sump pumps, factories, and so on. While comb and notch filters have proven effective in removing interfering harmonics in some cases they are suitable only to the more consistent sources in steady state conditions. In an exercise at ERDC's Waterways Experiment Station in Vicksburg, MS. aimed at directionalizing regional fireworks during both New Years and Fourth of July celebrations, a substation and local traffic were observed masking weaker impulsive signals from smaller or more distant firework impulses. Even when weaker impulses were still clearly visible well above the noise floor in the time domain signals, cross-correlation peak extraction would often indicate the continuous sources due to their higher power even in smaller correlations windows.

(U) In an effort to develop a fast sliding-window based detector as part of weak impulse localization in the presence of continuous background noise, a processing code was developed aimed at capturing the broad band spectral contributions of a weak impulse such as those from small munitions. Since any window large enough to capture element delays across the array will inherently also capture multiple cycles of any high frequency continuous sources, those continuous narrowband sources will have relatively high and narrow spectral peaks corresponding to their fundamental and harmonic frequencies. Impulse sources without excessive levels of dispersion caused by long range propagation will tend to be much more broadband and contain relatively high frequencies and a relatively low quality factor. A linear fit on the array element averaged spectral floor of the sliding windowed signals was performed by amplitude threshold limiting the spectrum to one half or less the peak amplitude of the highest signal. Spectral points whose amplitude was higher than the aforementioned threshold were omitted from the curve fit via not a number (NaN) substitution in Matlab. The resulting line fit was a fair approximation to the spectral floor of the averaged five arrays. In the presence of a weak impulses with minimal dispersion the slope of this linear fit tilts up and the y intercept moves down. The slope of this line serves as a first stage detector for weak impulses. The red line in the bottom left of Figure 3 shows the line fit in the presence of the continuous noise and no impulse present. The red line to the right in the lower graph of figure 3 shows the positive slope and offset change that occur when firework impulses are present in the spectrum. This detector is considered a first stage detector as some high frequency sources such as close proximity high speed moving vehicles did pass the detector slope criteria when it was set to the lower slope threshold levels. Directionalized fireworks results are shown in Figure 4. These are grouped according to signal amplitudes and identified in the figure's description. More dispersive sources, such as large munitions at longer propagation ranges could also be covered by this approach by additional spectral floor fitting. This continuous source removal was also evaluated using adaptive recursive narrow band filters to remove the continuous noise sources and leave just the spectral floor for cross-correlation based estimation. In this more sophisticated version the correlation aligned signals were processed with the iterative and FASTica Matlab algorithm developed by Hyvarinen and colleagues [4]. This independent component analysis code performs blind source separation and was able to successfully isolate the impulsive source from the nearby substation transformer hum present in the focused signals. This produced an optimized realization of the impulse. The main limitation of ICA seen in tests with SIAM data is that it is not able to account for time delays and therefore only produces channel amplitude scaling vectors to separate sources.

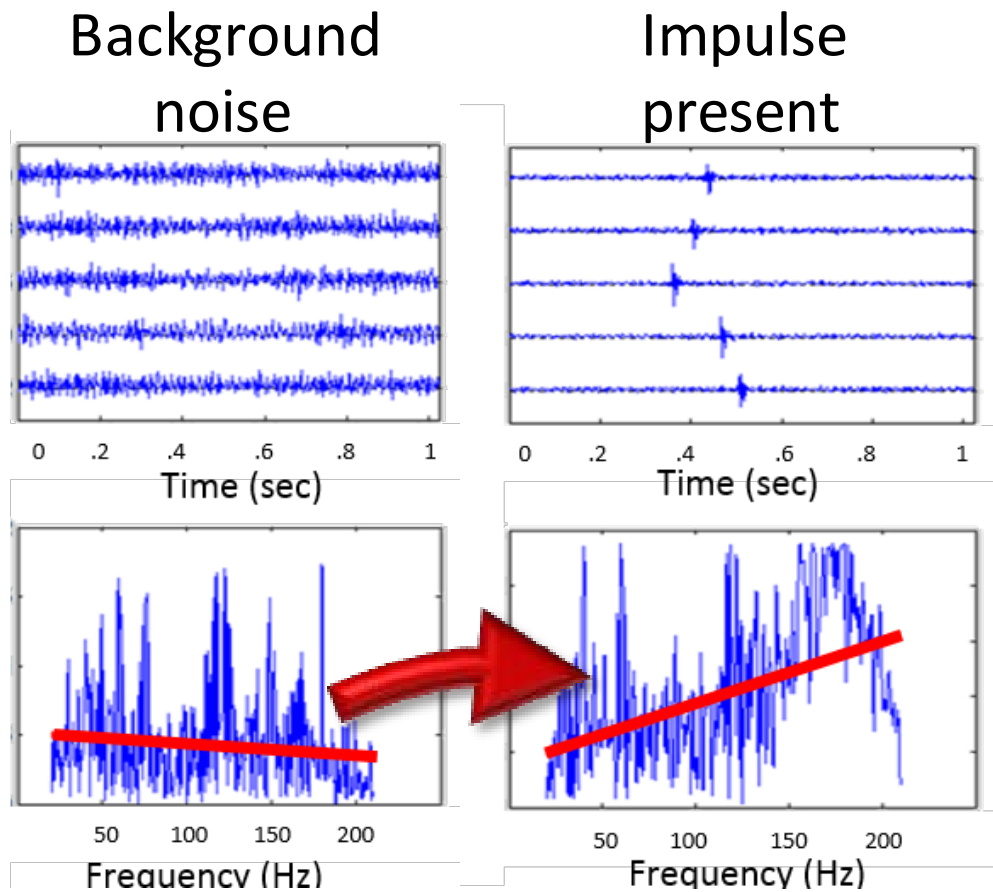


Figure 3 (U) The two left panels show array time signals (top) and their composite frequency (bottom) with only ambient background noise present. To the right of those two panels data is shown with an impulse from a small regional firework. The presence of the impulse raises the spectral floor's linear fit slope and shifts its offset (red lines). The slope and offset of the spectral floor data fit are then used as a first stage impulse detector for weak impulses embedded in the presence of continuous noise. Vertical axis units were not shown as figures are highlighting relative shape.

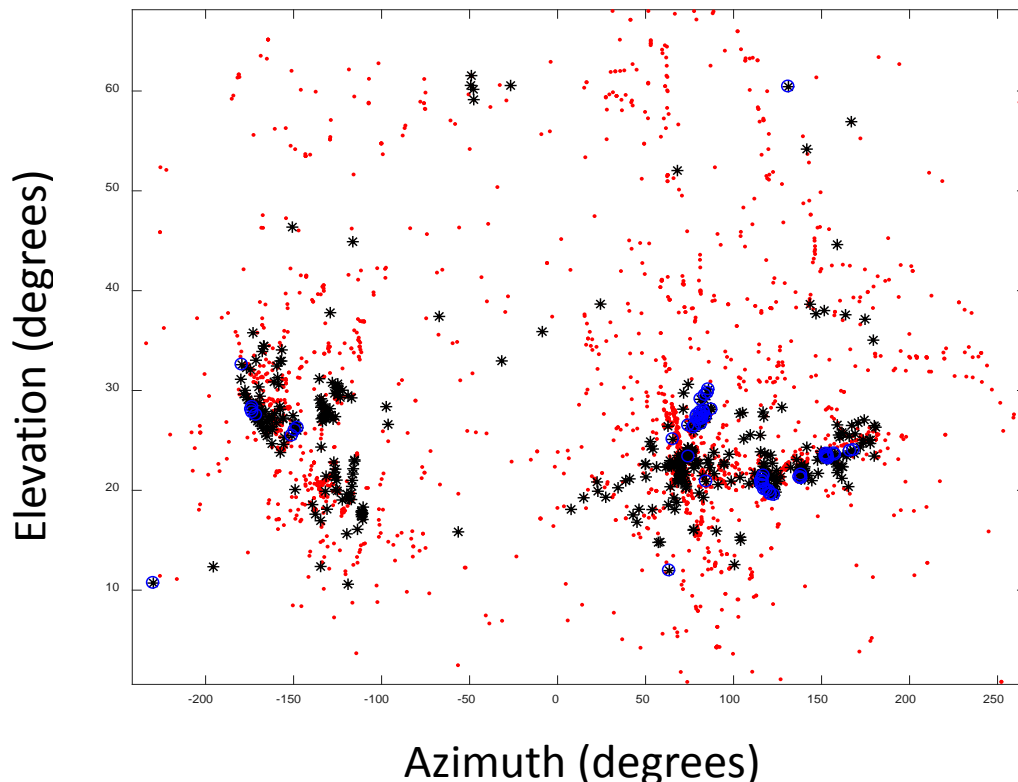


Figure 4 (U) Elevation versus Azimuth DOA plot for one hour of high activity local neighborhood fireworks detected by the stage one detector set to a minimum threshold. Higher energy events are marked in blue, medium events in black, and the smallest events are indicated with red dots. The detector's slope threshold was set low in this example.

(U) 2.2 DOA estimation using a neural network based fitting function

(U) In the initial mortar launch and impact location effort [5], direction of arrival estimation was first performed by ignoring elevation and locating only the azimuth of arrival. In order to extend capabilities a lookup table of array specific expected delays was developed by forward modeling with Matlabs Phase Array Toolbox. The resulting lookup table performed well in directionalizing cross-correlation and other delay results however investigated search methods were all slow due to map size and dimension. The solution to this problem was to develop a neural network based fitting function also trained to be resilient to cross-correlation noise occurring with low SNR signals.

(U) The fitting function was designed as follows. An array channel map spreadsheet is selected that defines the array's geometry in GPS coordinates. These are converted to meter offsets from the array's center element. The Matlab's phased array toolbox functions are used to develop a delay vs arrival map using a forward geometric model and propagating wavefront. The resulting element delay map as a function of azimuth and elevation is perturbed with random noise levels applied as random percentage

offsets to random elements. The general noise added to the training data is along the lines of the following scheme:

- none of the channels affected for 70 percent of the data
- one of the channels selected randomly with up to 10 percent offset and for 10 percent of the data
- one of the channels selected randomly with up to 50 percent offset and for 10 percent of the data
- two of the channels delay sign and value changed randomly 5 percent of the time.
- all of the channels up to 2 percent random offset (each) for 5 percent of the data

(U) Without the necessary addition of noise, these neural networks will fail by large margins for very small deviations in the input delay estimation. The noise block above is a work in progress as it is still a slow process for feedback of results. This training process is a one-time occurrence unless performance is inadequate, sensors are moved, or convergence fails to occur. The training of the network generally takes no more than a few hours, to date convergence and performance have been good. Performance is monitored during training as is customary by retaining a significant fraction of data (10 to 25 percent) from the training data and using it for periodic evaluation during and after training. In comparison timing test this function ran 200 times quicker than searches of the model data. This process was automated to create stand-alone Matlab callable fitting functions with a standardized array naming scheme. During initial development, the neural network fitting function was compared to direction of arrival tools in the phased array toolbox, Frequency and wavenumber azimuth extraction results [6], as well lookup results and found to compare well. The additional speed over these other methods allows faster real time processing of the windowed signals. An example is provided using one of the arrays of the Feather River Bridge experiment located on the grounds of the small regional airport. To evaluate the neural network fitting function performance, it was provided standard cross-correlation delay estimates determined from a sliding cross-correlation window analysis and the resulting azimuth results were compared to the much slower frequency-wavenumber (F&K) peak locations. These results are shown in the bottom graph of Figure 5 with red points marking the F&K results and the Blue and Green dots representing two realizations of trained fitting functions. The top graph in Figure 5 shows the neural network's elevation results as a function of azimuth for the same airplane flyover event.

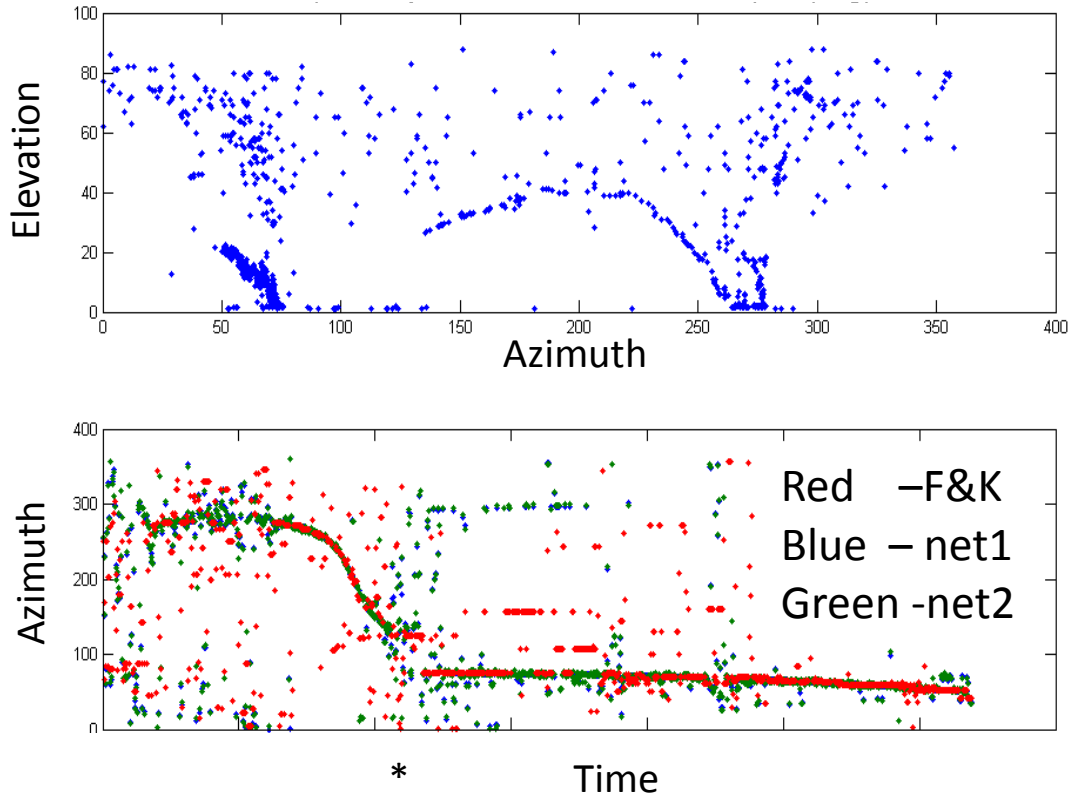


Figure 5 (U) (Top) Elevation vs Azimuth data generated from the neural network fitting function as a plane flies over the array. (Bottom) Azimuth vs time Neural Network fitting functions (blue and green for two trained version) compared to F&K determined azimuth data (red curve bottom graph).

In using various realizations of sliding window channel cross-correlations with low SNR sources, some benefit has been observed in analyzing the full cross-correlation delay matrix. With all delays referenced back to the central sensor statistical analysis has shown to be helpful in refining delay estimates. The even array symmetry used in the SIAM array also presents some additional opportunities for simple array correlation check and refinement as the center referenced channel delays should generally sum up to near zero with symmetry. Exact summation ranges can be extracted from the forward model. This property has been combined in code with another variation that includes utilization of the mode statistical function. The mode function returns the array element value that occurs most often and optionally counts the occurrences. In a high SNR case, a common channel referenced delay matrix will contain identical rows. Poor correlation points affecting only one or two channels can be mitigated in this way. The mode number can be returned with this function and has been used to provide feedback on how well the event tracked across the various combined correlation observation in the full matrix cross-correlation. Generalized cross-correlation variants such as the phase amplitude transform, maximum likelihood, Scott, and so forth are generally better suited to higher SNR conditions. Preprocessing signals prior to correlation is generally necessary for optimum performance. A wide array of conventional, adaptive, and non-linear filters have been explored in this respect. Removing any offsets, normalizing dataset amplitudes across channels, and resampling to a higher sampling rate are generally good first steps. One interesting preprocessing tool written in Matlab

and contained within the LANL software InfraMonitor 3.1 [6] is a nonlinear filter called the pure state filter. This filter is designed to remove frequencies not present across all channels in the windowed section. With the right input parameters and occasionally necessary windowing it has shown promising results on several datasets.

(U) 2.3 Localization across multiple arrays

(U) Once direction of arrival is made from multiple array locations, the detections should be checked to validate that the observed time difference of arrival matches in reasonable bounds with the delay predicted by propagation. Tools within the Matlab Mapping toolbox are used to generate an intersection point GPS point, and then path length differences between the arrays can be converted to propagation time. The relative time difference of arrivals are compared within a roughly 25 percent window to allow for topography, weather, and location uncertainty. Depending on the nature of the event and the degree of signal dispersion observed between arrays, the signals can be cross correlated to further extract the source signal from the background noise. Figure 6 shows detections from three arrays, with two arrays being used to triangulate the location of the cold gas thruster blast at the Portuguese Dam in Puerto Rico. This ongoing effort led by Henry Diaz at the ERDC Waterways Experiment Station in Vicksburg, MS., used an impulse source in 2016 to study the Dam's vibrational response. The local environmental background noise from the highway was also captured in the detections. The colored and brown translucent bands in the bottom two images are spatial histograms of detections from the southern array occurring in the same general time windows as the CGT blast events. The cars appear most detectable as shown in this spatial histogram (two bottom images) when they are undergoing high speed path deflections caused by turns in the highway, these cause rapid and spatially localized far field Doppler changes that are well suited for detection and localization with cross-correlation providing interference is minimal.

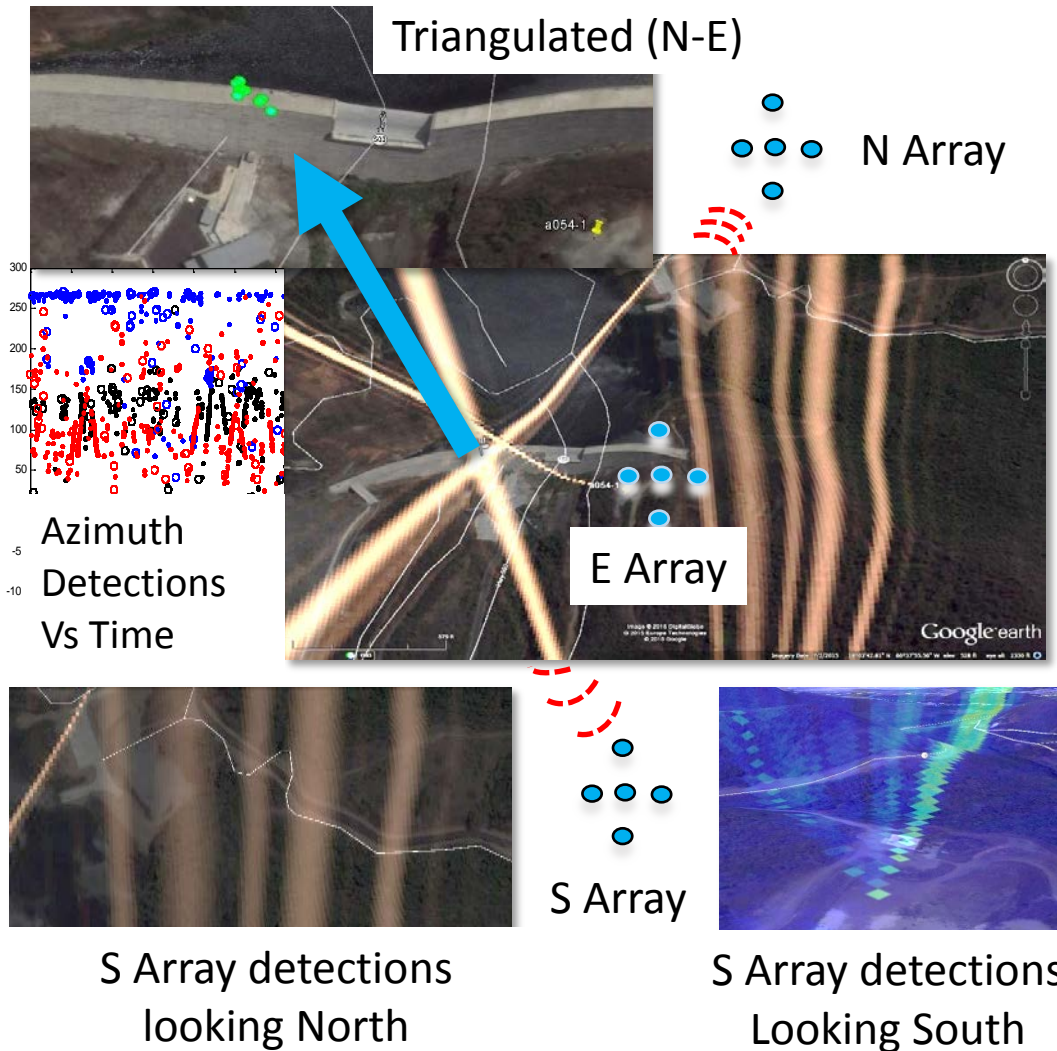


Figure 6. (U) Detections triangulated marked as green dots (top image) and validated using time difference of arrival. Detections illustrated with a spatial detection histogram (bottom three images).

(U) 3.1: Continuous noise sources, localization using modified cross-correlation

(U) In the experiments with weak impulses discussed in the previous section the operations of the cross-correlation function were modified in an attempt to better detect weak impulses in the presence of higher average power noise. In those modifications for impulse detection, the shifted cross-correlation vector product was replaced with an alternative vector formed by removing the negative components (by setting them to zero) and then the sign restored based on the input reference signal's sign. This resultant vector was reduced to a scalar for its shift point value, not by the usual summation process but by using the maximum-minimum values of that vector product. This change made the delays estimated from the peak locations sensitive to the maximum peak to peak signal amplitude vs average power. Based on the improvements of this variation for impulse localization in the presence coherent

noise, other variations that might improve cross-correlation performance in specific conditions were considered for continuous sources. In general cross-correlation performance is known to degrade on narrowband signals with cycle self-similarity. In an attempt to reject false cross-correlation delay estimation points that occur due to improper phase cycle locking, additional product vector variations were explored. While a number of statistical functions were explored on the product vectors, one of the promising approaches, was to sum the standard positive vector products and divide this by the sum of the negative vector products. For several continuous input signals with typical source variations and harmonics, this method appeared to provide additional phase cycle discrimination capability over conventional summation. The positive to negative ratio alternative to summation, which itself is a difference of the total positive and total negative product vector components, appears to provide greater alignment penalties when picking between similar cycles of the continuous source for the cases tested. The merits of this approach as well as its relevancy to frequency amplitude scaling and other extensions of generalized cross-correlation are still being explored. It can be seen in Figure 7 that the standard cross-correlation delay results (third panel down) fail to correctly identify array element delay values over significantly more data points than the alternative polarity ratio method (second panel down) that is described above.

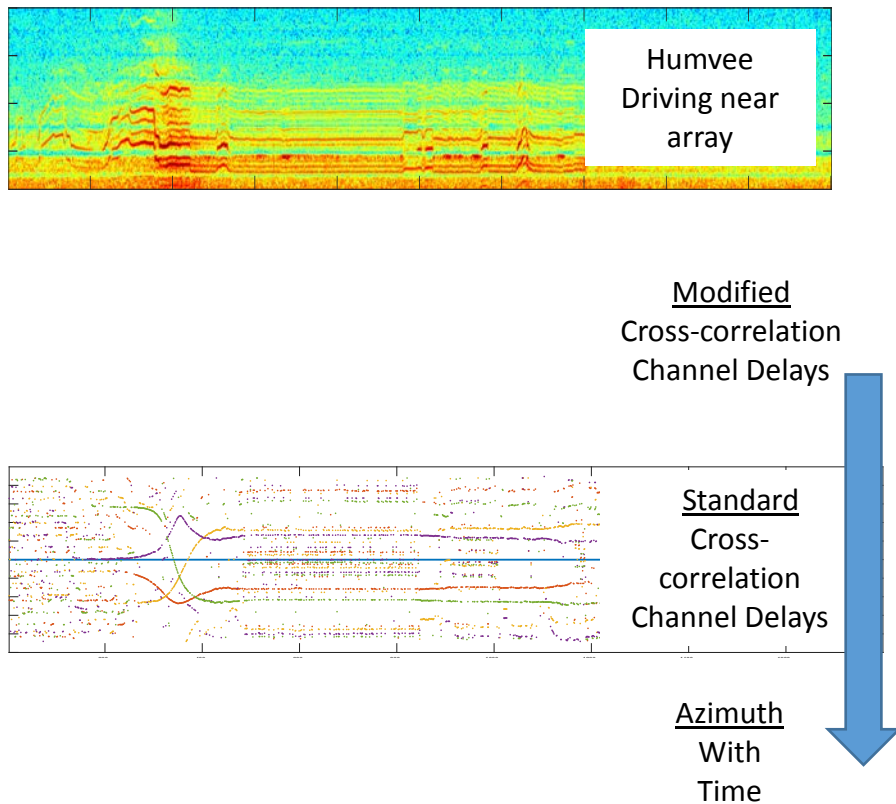


Figure 7 (U) Example of the modified cross-correlation results. Top panel is STFT of the slow moving harmonic source seen at one array element, note that this signal has had a comb filter applied to remove the interfering local gas generator. The second panel shows channel delays vs time using the modified method with the results of the standard correlation process being shown in the third panel for comparison. The final panel shows resulting azimuth determination using the neural network fitting function previously described.

(U) 3.2 Tracking relative instantaneous frequency to find direction of arrival

(U) In an effort to more robustly characterize the direction of arrival of source observed frequency chirps, frequency and phase tracking experiments across the array have been performed. These investigations led to an evaluation of relative instantaneous frequency as a potential supplementation to the cross-correlation and adaptive beamforming approaches that are also being considered in this project. The idea, applied to other systems by [1] [2] and presented more primitively here, is that as a frequency change such as an RPM or state change on a stationary piece of equipment or a Doppler or RPM based chirp from a moving source will produce frequency tracking features as the chirp propagates across the array elements. In order to best capture these features, the central array element's instantaneous frequency or phase is subtracted from the outer element's instantaneous frequency or phase. This relative frequency for the outer elements should generally be proportional to the chirp's rate of change and affect the various outer array elements according to the direction in which the chirp is propagating across the array. Figure 8 top panels show a set of relative (to center channel) phase angles of a synthetic chirp as it propagates across the array from 15 different simulated directions of arrivals. This first study with synthetic noise found the method's SNR limitation to be proportional to the sources frequency rate of change, which is logical. Gaussian noise was added to the synthetic signals to determine SNR limitations when using the based Hilbert phase angle extraction and comparison. A SNR of .7 was required to localize chirps changing at a rate of 10 Hz/second, while a SNR of 4 was required for slower chirps with a frequency change rate of 1 Hz per second. Classical issues with phase unwrapping via amplitude based switching, a high sample rate demand, and the need to take the derivative, led to a move to high resolution STFTs for further field data investigations.

DOA / channel study for chirp (no noise example)

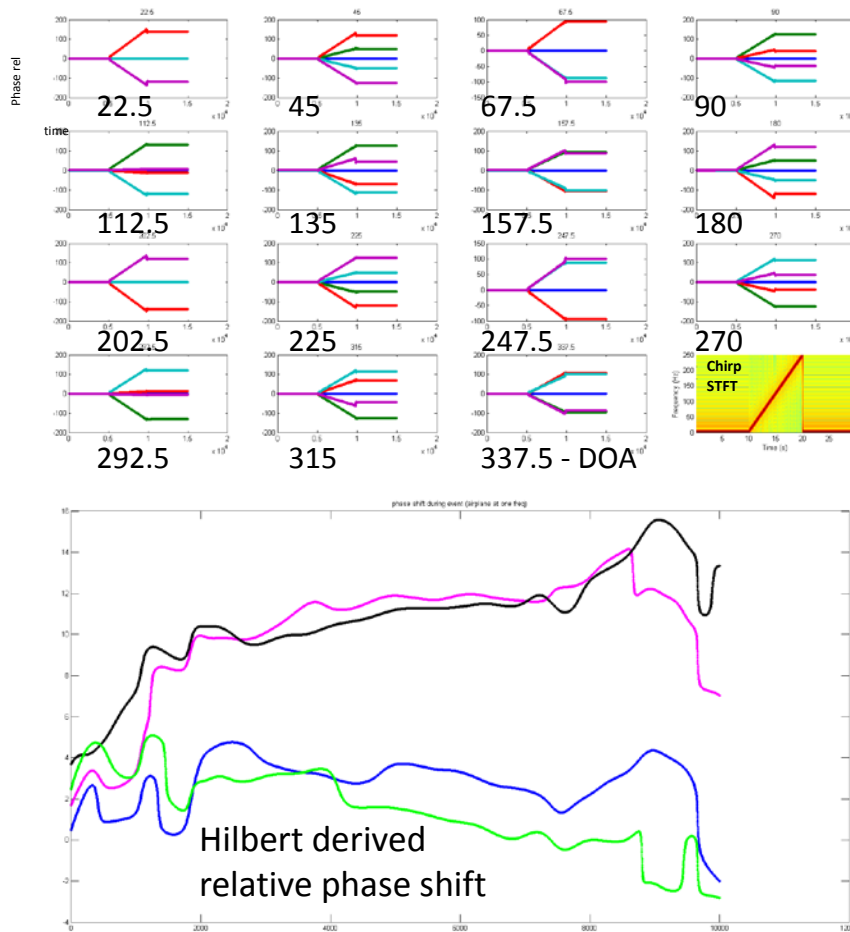


Figure 8 (U) (Top) Synthetic chirps and the Hilbert transform were used to evaluate phase angle rate of change as a method to determine direction, SNR performance was evaluated by addition of noise. Each of the top 15 panels show different directions of arrival and the resulting unwrapped relative phase angle change for a linear chirp. Azimuth Direction of arrivals in degrees are shown under each graph. (Bottom) Variations in instantaneous relative frequency first observed in field data by means of the Hilbert transform's relative unwrapped phase angle.

(U) A distance normalization scale was created for ranging the sensors x and y locations and to help compensate for imperfections in the array's field placement. Essentially this is a channel multiplier that normalizes sensor error placements so that closer elements in both x and y are compensated for in the frequency shift comparison. This multiplier is applied to the relative frequency vectors which are used to estimate direction of arrival in the same general way that delays are.

(U) The current direction of arrival estimation from this process takes into account the source's frequency direction of change. An averaged frequency composite across channels is smoothed and its derivative taken to develop a multiplication vector for frequency rate scaling and polarity correction.

The rate/polarity scaling vector has the additional capability of essentially turning off the algorithm if the signal is not increasing or decreasing sufficiently for lead/lag detection. Refinement of this weighting function is still under development and the results presented here only include single value polarity compensation applied to mostly one directional chirps. Some initial test with data showed that the rate/scaling function applied to each time instance was able to retain source direction for chirps that changed frequency direction one or more times.

(U) In general the current non-optimized implementation process is as follows. A small frequency chirp is identified for analysis from a larger STFT by dragging a GUI box around it, and a very high resolution STFT for the region of interest is collected for each array channel. Currently this STFT is using a blackmann-harris window with a length roughly six times the array's delay aperture. A STFT mask is applied based on taking the log product of all SFTFs, image thresholding that data, performing object detection, and taking the largest object as the STFT mask. This serves to minimize interference from other frequencies and noise sources that might also be in the selected analysis window. The frequency peak is located and stored as the instantaneous frequency for each channel as a function of time. The relative frequencies are generated by subtracting the four outer channels from the center element. This is multiplied by the polarity and scaling vector described in the previous section (scaling factor not included in result here). A version of this matrix is optionally smoothed to improve angle determination in low SNR cases. The leading and lagging frequencies are used in a Cartesian scaled reference to determine direction of arrival as a function of time. The relative frequency of array elements opposite each other on the coordinate axis are subtracted to determine the proportional x and y coordinates. These are then transformed into polar coordinates for estimating azimuth. Doppler dominated or Doppler near field described in the paragraph below, may need propagation model refinement for DOA estimation.

(U) An observation was made first with cars on a busy street near a deployed ERDC array and later in other datasets such as planes in the Feather River bridge experiment. The Feather River Bridge Experiment is part of the structure based acoustics research being performed by ERDC [7]. In Doppler events where the source is close to the array or moving at high velocity, the extracted frequencies can be seen shifting by more than the array's delay aperture. It is thought that this is most likely tied to the Doppler Effect and each sensor having a slight variation in its time and frequency response due to Doppler observer differences at each sensor's position. This effect is visible on close traffic and more distant sources traveling at high velocity. State changes on stationary equipment such as sump pumps operating near the array or more distant moving sources, do not appear to exhibit these larger than expected time shifts. This apparent element delay beyond the array's maximum delay aperture appears to explain cross-correlation failures when the source is close and/or moving fast and signal self-similarity is not an issue (see asterisks in Figure 5).

(U) A SIAM array was deployed on the grounds of the Marysville Regional Airport in California, this array was located several hundred yards to the west of the southern end of the runways. Results from a propeller based plane flying near the array at the Feather River Bridge Experiment Airport located Array are shown in Figure 9. Also shown for this example is the larger and lower resolution STFT (top center image) used for chirp selection. A box selection is used to define the time and frequency limits for the analysis STFT. The selected chirp is shown as a short time frequency transform in the top right panel of Figure 9. A masks is applied following detection of the highest amplitude frequency at each time instance for each channel the resultant frequencies can be seen the top left graph of Figure 9. It can also

be see here that the time separation is 1.3 seconds, is much larger than the maximally .2 sec delay aperture. Taking the relative frequency to the center channel produces the curves shown in the bottom right which lead or lag by no more than 3 hertz. Because the array elements are essentially lying on a Cartesian grid the relative frequency leading and lagging can be used to gauge location respect to time. It is possible that this model may need refinement in the near-field with observable Doppler effects. In the case of the nearby road covered in the next example this effect was observed at distances around 0.1 miles or 160 Meters.

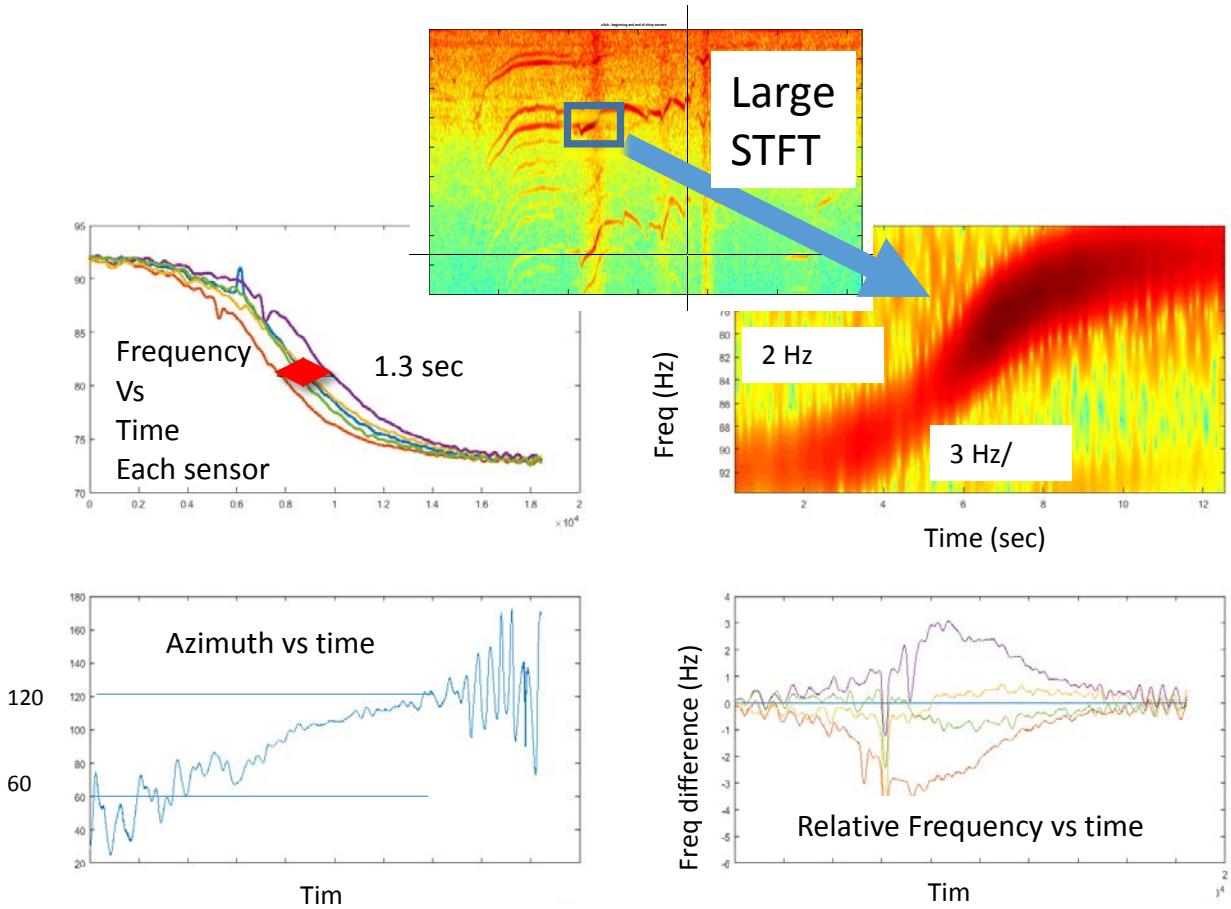


Figure 9 (U) STFT (top center) A GUI box is used to select the source chirp for analysis. (top right) The high resolution STFT is calculated for each array element and (top left) the maximum frequency is determined after applying an STFT mask, The relative frequency (bottom right) is used to quantify the frequency leading and lagging across the array as a function of time. An azimuth vs time plot is generated based on the relative frequency shifting.

(U) In Figure 10 below a similar set of graphs for a car driving on an adjacent road near a temporary array set out at ERDC Vicksburg are shown. No data smoothing was applied in this example or the less

noisy previous example shown in Figure 9. Doppler observer influences are seen again in this example where the source is moving slower, but much closer to the array. In this case the frequency propagation delay in the upper left graph of Figure 10 is roughly .8 seconds or 4 times the expected maximum delay across the array (note that this is zoomed into the higher slope section of the chirp). For the case of this lower

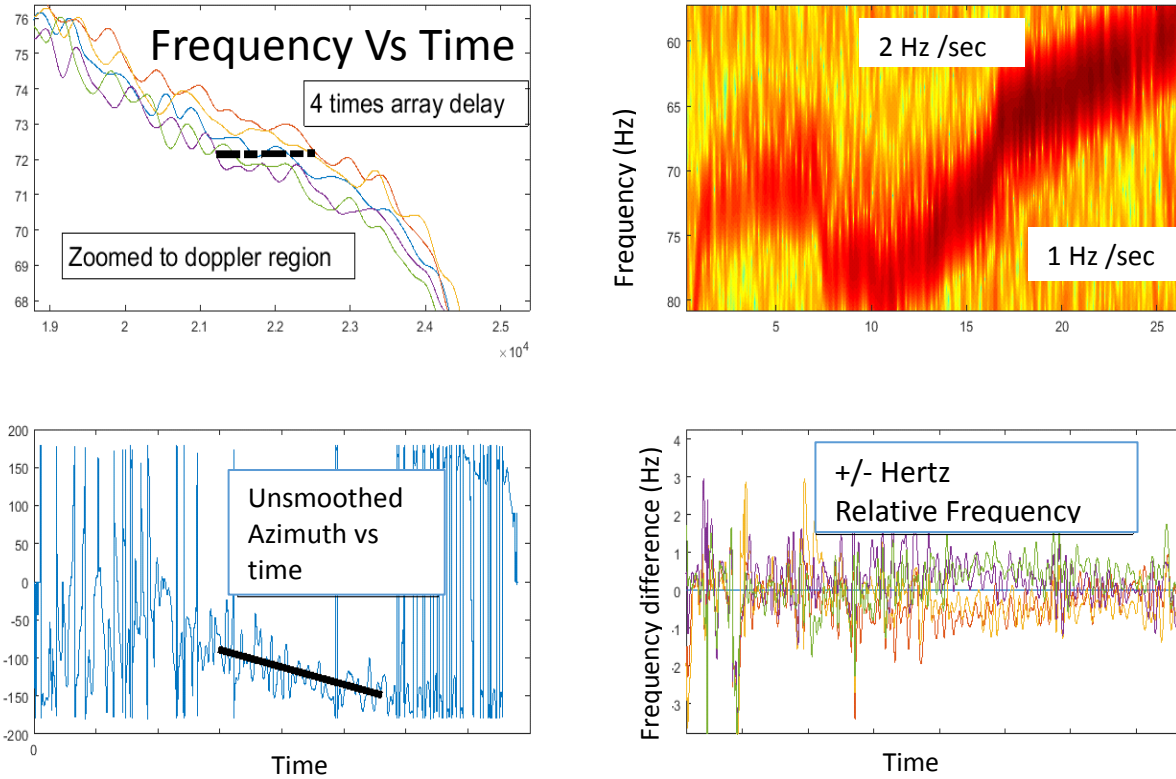


Figure 10 (U) A noisy chirp example that also shows significant detection of Doppler influences. Note that this version has smoothing turned off so that current failure over slower changing and lower SNR sections of the STFT can be illustrated. These failures are observed in the bottom left panel to the left and right of the diagonal black line.

(U) SNR case it appears that a frequency rate of change of 2 Hertz per second produces detectable relative frequency differences, while 1 Hertz per second does not. The averaging function has the capacity to improve the range but should be applied after data validation. The source over the higher chirp rate section of the signal using the present model appears to moving from -90 to -150 degrees in azimuth. In the earlier cross-correlation and F&K data shown in the bottom graph of figure 5 we can see both the cross-correlation and F&K approach fail at the peak Doppler transition moment (around the sliding window data point labeled with the asterisk on the horizontal axis). The larger than expected time delay between dominant like-frequencies is thought to be the possible cause of this.

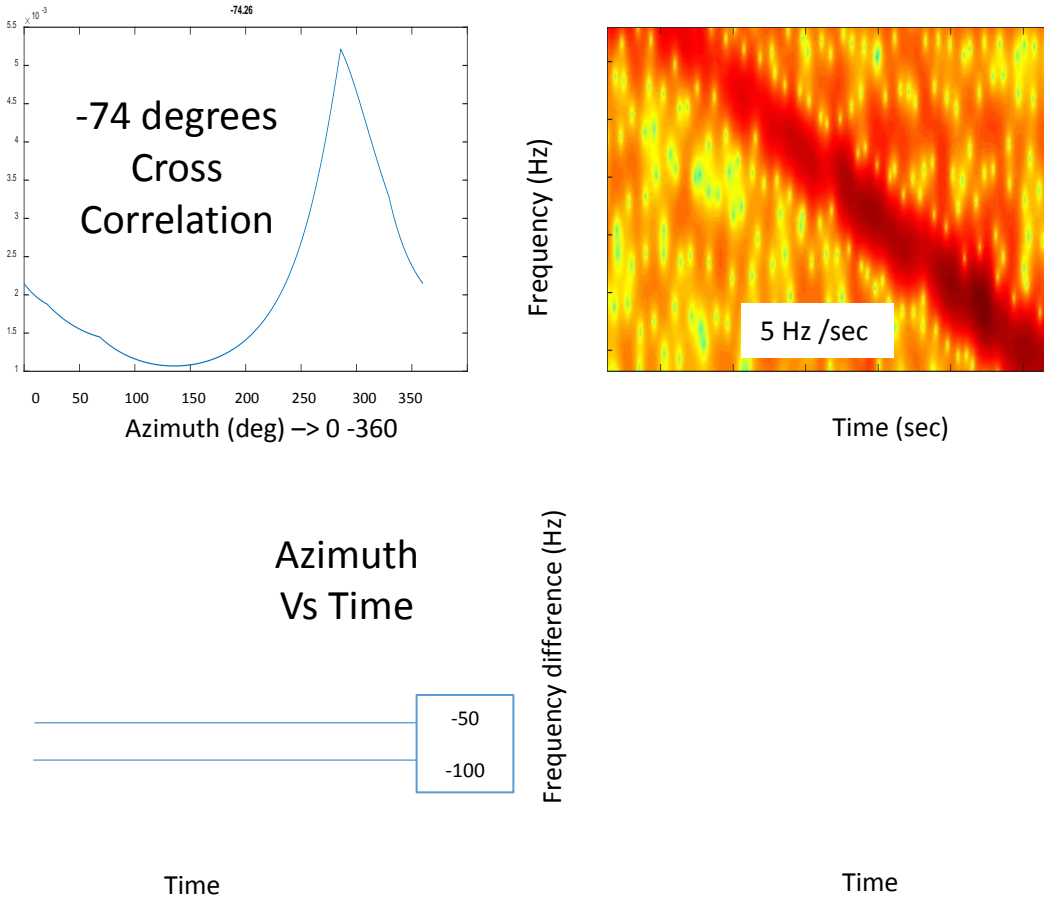


Figure 11 (U) Comparison of a cross-correlation based direction of arrival (top left figure) with the method presented in this section using relative frequency with two levels of smoothing (bottom left). Observed time delays were within range of the delay aperture as indicated by the good correlation and LMSE based DOA peak in top left figure.

(U) The relative frequency lag method for chirp localization presented here was compared with cross-correlation over a number of chirps using both short and long windows. The long windows perform better but provide only a single data point. Cross-correlations were performed on the bandpass filtered data and time windowed data so that the same data was being processed. The exception would be any noise points removed by the STFT masking. In general cross-correlations compared well with the method presented here. The exceptions were generally the noisier data and the data with time delays beyond the expected maximum array delay values. An example of the agreement with the two approaches is shown in figure 11. The cross-correlation based LMSE approach located the source at -74 degrees Azimuth (or 286 degrees shown on the top-left graph). The frequency difference approach (bottom left) showed good agreement over the valid frequency separation range shown in the bottom-right graph of Figure 11. In the lower left graph of Figure 11 a low level of smoothing of the relative frequency used for direction estimation is shown with the blue line and a higher level of smoothing is shown with the red line.

(U) 4 Results and Conclusions:

(U) A wide variety of acoustical sources exist in urban environments. Optimum utilization of multiple large aperture infrasound and acoustic arrays in or near urban spaces requires an understanding of various sources being received and their characteristics and origins. This is true whether those acoustic sources are of interest or not. A variety of detection and localization strategies for weak impulses and continuous sources has been presented in this paper. Various modifications of the cross-correlation process have been demonstrated to be useful for improving delay estimation results for both impulsive and continuous signals in at least certain cases where conventional cross-correlations preprocessing can be no further improved. An approach is also presented to allow automated training of a neural network fitting function to perform the mapping between a given sensor array's channel delays from cross-correlation or beamforming and the resulting azimuth and elevation direction of arrivals. This method requires some initial training time but once trained delays can be resolved at much higher speeds and with reasonable immunity to cross-correlation errors. A quick example of triangulated data using two arrays is also presented as this is the ultimate end goal of multi array deployments such as the SIAM system and DOA estimation. Lastly a method to localize sources based on array propagation of their observed frequency chirp characteristics is presented. This method which is still in early investigative stages here, appears to have some supporting value to cross-correlation and possibly nearfield or Doppler event isolation. While the experiments presented here agreed with cross-correlation results and generally pointed in expected directions of proximal roads and other known sources, more controlled pilot studies are needed for model refinement. The tools presented here will be refined and integrated into the SIAM monitoring system contingent on their performance in continued evaluation and refinement efforts.

(U) References:

[1]

Ma, N. Goh J.T., Ambiguity Function based Techniques to estimate the DOA of Broad Band Based Chirp Signals, IEEE Transactions on Signal Processing, VOL 54 No 5. May 2006.

[2]

Abadi, S.H. Blind deconvolution in multipath environments and extensions to remote source localization, PhD Dissertation. ME University of Michigan, 2013.

[3]

Comon P Jutten J. Handbook of Blind Source Separation, Independent Component Analysis and Applications, published by Academic Press, 2010

[4]

Hyvarinen, A. Sarel, J, Hurri, J, Gavert, H. [software] FASTica available for download from:
<https://research.ics.aalto.fi/ica/fastica/>

[5]

Mckenna, M, Haskins, R.,Carbone, C. Simpson, C., (UNCLASSIFIED) Real-time DCL of Mortar launch and impact using SIAM . Proceedings of the 2014 Military Sensing Symposium: Battlespace Acoustic, Seismic, Magnetic, and Electric-Field Sensing and Signatures. 28-31 October 2014. Springfield, VA.

[6]

Arrowsmith, S, Marcillo, O. *Inframonitor* (2012) 3.1, *Los Alamos National Labs* [software] available for download from: <http://www.lanl.gov/projects/inframonitor/index.html>.

[7]

Whitlow, R.D., A.M. Jordan, S.L. McComas, H. Diaz-Alvarez, and M.H. McKenna (2014). Structural Infrasound: A scour case study of the Feather River Bridge. Proceedings of the 2014 Military Sensing Symposium: Battlespace Acoustic, Seismic, Magnetic, and Electric-Field Sensing and Signatures. 28-31 October 2014. Springfield, VA.